CRYSTAL GROWTH & DESIGN
2003
VOL. 3, NO. 5
727−731

Relating Microdefects to Growth Conditions in Czochralski Si Crystal Growth

Axel Voigt* and Christian Weichmann

Crystal Growth Group, Research Center Caesar, Ludwig-Erhard-Allee 2, D-53175 Bonn, Germany

Received January 15, 2003; Revised Manuscript Received May 21, 2003

ABSTRACT: The formation of grown-in defects in silicon crystals is controlled by the concentration of intrinsic point defects. Under steady-state conditions, the type of the prevailing point defect species is linked to the ratio of pull rate (v) and temperature gradient (G) in the crystal at the solidification front. It has been shown that this ratio as well as computed point defect distributions are in good agreement with experimental data. In this paper, we couple transient heat transfer with transient point defect models and show that the quasi-steady assumption and the v/G criteria are no longer valid if strong variations in the pulling velocity occur. Therefore, for a detailed understanding how defects are related to growth conditions, the thermal history should not be neglected.

Introduction

Today, it is well-known that the concentration of intrinsic point defects in a growing silicon crystal can be qualitatively explained as a function of the pulling rate v and the temperature gradient G at the solidification interface. At a critical ratio of $v/G = 1.34$ mm^2/K min,[1] interstitials and vacancies annihilate each other, and the crystal shows neither dislocation loops nor voids. Below that critical value, interstitials dominate, and at higher values vacancies are in excess. The v/G theory assumes steady-state conditions during the whole growth process. For grown-in defect formations, this is realized when the pull rate remains constant during the growth until the crystal has reached a temperature of approximately 1200 K. This defect formation has been extensively studied experimentally and theoretically for almost steady-state growth conditions. For widely varying growth conditions, it has been shown that the v/G criteria as well as computed point defect distributions are in good agreement with experimental data.

In this paper, we solve a coupled transient heat transfer and transient point defect transport model and demonstrate that Voronkov's v/G theory[2] is no longer valid for strong transient effects such as variations in the pulling velocity.

Multiscale Model. The different length and time scales in Czochralski (CZ) silicon crystal growth lead to a hierarchy in the developed model. Heat transfer and point defect transport are coupled only in one way. Point defect dynamics are highly dependent on the temperature in the crystal, but because of the low intrinsic point defect concentrations they do not influence the heat transfer in the crystal.[3]

Heat Transfer. Heat transfer in a Czochralski furnace occurs by conduction, convection, and radiation. The equations for the temperature are

$$\rho_{0\mathrm{i}} c_{p\mathrm{i}}\left(\frac{\partial T_\mathrm{i}}{\partial t} + u_\mathrm{i}\cdot\nabla T_\mathrm{i}\right) - \nabla\cdot(k_\mathrm{i}\nabla T_\mathrm{i}) = \rho_{0\mathrm{i}} P_\mathrm{i}$$

where $\rho_{0\mathrm{i}}$ is the density of the component, $c_{p\mathrm{i}}$ is the heat capacity, u_i is the velocity, k_i is the thermal conductivity, and P_i is a heat source term. The index i indicates the different components of the apparatus, such as melt, crystal, crucible, heaters, heat shields, and insulators. The heat sources P_i are nonzero only in the heaters. Convection in the melt is governed by the Navier−Stokes equation

$$\frac{\partial u_\mathrm{m}}{\partial t} + (u_\mathrm{m}\cdot\nabla)u_\mathrm{m} - \upsilon\Delta u_\mathrm{m} + \nabla p = \beta(T_\mathrm{m} - T_0)g$$
$$\nabla\cdot u_\mathrm{m} = 0$$

where u_m is the velocity, p is the pressure, and T_m is the temperature, and where the melt is Newtonian and variations of melt density are negligible, except in the calculation of the body force induced by thermal buoyancy, which is the onset of Grashof convection. The influence of the gas flow is neglected. Further, it is assumed that no radiation is emitted or absorbed by the gas and that radiation is only diffuse. Moreover, it is considered that emission, absorption, and reflection of radiating waves occur only at the surfaces. The heat balance at the surface relating the heat flux caused by conduction to the surface q, the radiosity, and the irradiation then becomes $q = G(\sigma T^4)$, with $G = (I - \epsilon K(I - (1 - \epsilon)K)^{-1})\epsilon$. σ is the Stefan−Boltzmann constant, ϵ is the emissivity, and the operator K is defined as

$$K\lambda(r) = \int_\Gamma \omega(r,s)\Xi(r,s)\lambda(s)\,ds,\ \forall\ r \in \Gamma$$

where Ξ(r,s) is a visibility factor. Along the free melt-crystal interface mass conservation and a no-slip boundary condition are valid. Due to the rotation of the crystal, this no-slip condition is the onset of forced convection by crystal rotation. At the melt-crystal interface two thermal conditions have to be specified, and $T_\mathrm{m} = T_\mathrm{c} = T_\mathrm{eq}$ is set, where T_eq is the equilibrium melting temperature. The second thermal condition takes account of the heat flux balance between the two phases, and the heat flux in the crystal is greater than in the melt by the amount of latent heat released during solidification, i.e.,

$$k_\mathrm{m}\nabla T_\mathrm{m}\cdot n - k_\mathrm{c}\nabla T_\mathrm{c}\cdot n = \rho_{0\mathrm{c}}\, l\,(u_\mathrm{c} - u_\mathrm{f})\cdot n$$

* To whom correspondence should be addressed. Axel Voigt, Crystal Growth Group, Research Center Caesar, Ludwig-Erhard-Allee 2, D-53175 Bonn, Germany. Web: http://www.caesar.de/cg. E-mail: voigt@caesar.de. Phone: 0049-228-9656236. Fax: 0049-228-9565111.

10.1021/cg034005u CCC: $25.00 © 2003 American Chemical Society
Published on Web 07/01/2003

where l is the latent heat, n is the normal vector, and u_f is the speed of the phase-boundary.

The meniscus separating the melt from the ambient gas is another free interface, whose shape is part of the problem unknowns. Here again a Boussinesq-type approximation is made, where it is assumed that the surface-tension coefficient γ equals a constant γ_0, except in the boundary condition for the tangential stress. The temperature differences at the interface have an influence on the transport of momentum and heat near the interface. The surface-tension gradient resulting from these differences acts like a shear stress on the melt–gas interface and thereby generates a surface flow. This phenomenon is known as Marangoni convection. It is assumed that the melt perfectly adheres to the crucible wall. A no-slip condition for the velocity is set at the crucible wall. This is the onset of forced convection due to rotation of the crucible. At the remaining boundaries, only conditions for the temperature have to be set. At the surfaces of the melt, the crystal, the crucible, the heaters, heat-shields, insulators, and the inner surface of the enclosure $k_i \nabla T_i \cdot n = -G(\sigma T_i^4)$ is taken, where i stands for the different components. Initial conditions for the temperature T_i in all components of the apparatus, conditions for the velocity u_m in the melt, and an initial domain for melt and crystal have to be described.

Point-Defect Dynamics. Point defects are incorporated into the crystal in their equilibrium concentrations and then diffuse and recombine rapidly in the high-temperature portion of the crystal. In the model convection, Fickian and thermodiffusion and reaction of point defects in the growing crystal are considered. Fickian diffusion is driven by concentration gradients in the crystal, and thermal diffusion is driven by temperature gradients in the direction of increasing temperature. Recombination is characterized by the annihilation of interstitials and vacancies and the creation of an undisturbed lattice site. The governing equations for the concentrations of interstitials and vacancies are

$$\frac{\partial C_i}{\partial t} + u_c \cdot \nabla C_i - \nabla \cdot \left(D_i \nabla C_i - \frac{Q_i D_i C_i}{k T_c^2} \nabla T_c \right) = k_{rec}(C_i^{eq}\, C_v^{eq} - C_i C_v)$$

$$\frac{\partial C_v}{\partial t} + u_c \cdot \nabla C_v - \nabla \cdot \left(D_v \nabla C_v - \frac{Q_v D_v C_v}{k T_c^2} \nabla T_c \right) = k_{rec}(C_i^{eq}\, C_v^{eq} - C_i C_v)$$

where C_i and C_v are the concentrations of interstitials and vacancies, D_i and D_v are the temperature-dependent diffusion coefficients, Q_i and Q_v are the activation enthalpies for thermal diffusion, C_i^{eq} and C_v^{eq} are the equilibrium concentrations, k is the Boltzmann constant, and k_{rec} is the reaction coefficient for recombination. Clustering of point defects is not taken into account because the point defect concentrations already reflect the latter grown-in defect distribution. Dirichlet conditions with the equilibrium concentration are specified as boundary conditions along all crystal surfaces.

Numerical Methods. Coupled heat transfer and point defect equations are solved by finite elements. The discretization is based on the work in refs 1, 4, and 5

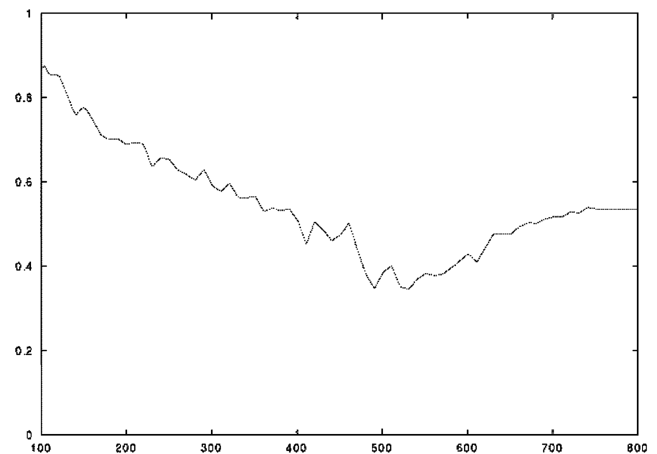

Figure 1. Velocity profile for growing process in mm/min over crystal length.

For the melt, the heat conduction equation has been solved by adjusting an effective heat transport coefficient inside the melt, which has been extracted from temperature measurements and melt flow calculations.[6,7] By this treatment, we can approximate the influence of the melt flow without explicitly calculating the melt convection, which would increase the computational effort dramatically. We are interested in a time scale of hours, which is much larger than the time scale for melt convection and as long as impurity transport is not a major concern; neglecting the melt flow can already reproduce experimental measurements in a satisfactory way.[8] Therefore, we only include convection in an averaged way by effective heat transport coefficients. The integral equation to model heat radiation is discretized by piecewise constant elements. The method of refs 4 and 9 is used to calculate the view factors in rotational symmetric domains. In most heat transfer simulation of Czochralski crystal growth processes, quasi-steady-state conditions are assumed. Transient simulations in which geometry changes due to the growing of the crystal are taken into account where previously performed by refs 10–12. For the simulation of point defects, the influence of thermal diffusion is neglected in the numerical procedure. A parameter set for diffusivities and equilibrium concentrations obtained by ref 3 is used for the calculation which describes grown-in defect distributions for a large number of crystals grown under steady-state process conditions for various hot zones and crystal diameters.[1] Due to different time scales for temperature and geometry changes and point defect dynamics, a coupling between this phenomena is not necessary in each time step. Point defect concentrations evolve much faster than temperature changes in the crystal; therefore, several time steps in the calculation of point defect concentrations are solved before the temperature and the crystal shape are updated. In previous transient point defect simulations,[13] the growing of the crystal and the temperature change during the growing process were not taken into account.

Results and Discussion

The simulations are performed for an experimental furnace to grow crystals with 200 mm diameter. The

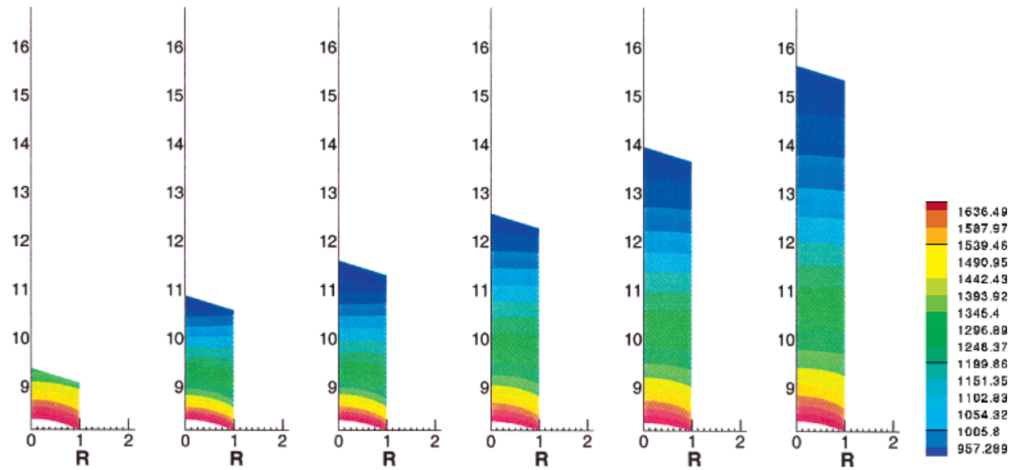

Figure 2. Temperature distribution in crystal at various time steps.

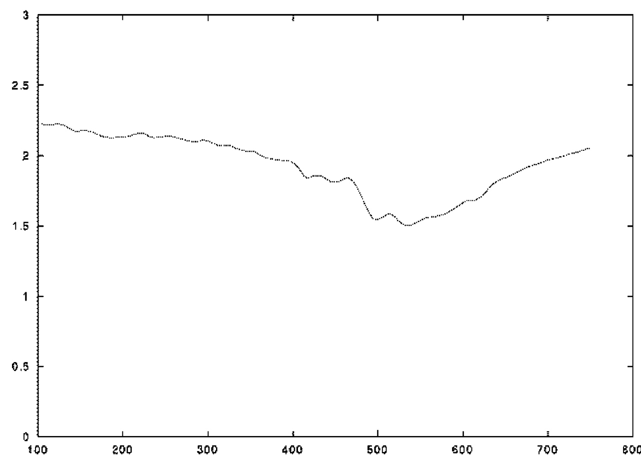

Figure 3. Interface deflection at center for growing process in cm over crystal length.

simulation start with an initial quasi-steady-state computation for a crystal length of 10 mm. The pull rate is in the range of 1 mm/min and is ramped down according to Figure 1. The simulation is performed until a crystal of 750 mm length is grown.

Temperature Distribution. The computed temperature distributions in the crystal agree well with our experience from temperature measurements.[6] The temperature profiles for various time steps are shown in Figure 2. The upper part of the crystal continuously cools during the growth process. The axial temperature gradient is larger close to the phase boundary and decreases with increasing crystal length. In contrast to the transient heat transfer simulations mentioned in ref 13, we observe a strong influence of the pull rate on the interface shape Figure 3. The deflection of the interface is directly related to the pulling velocity. Due to the sensitivity of the temperature gradients at the interface, the variations of its shape should not be neglected.

Point Defect Distributions. At the interface, interstitials and vacancies are incorporated at their equilibrium concentrations of 1.0×10^{-15} and 1.2×10^{-15} cm^{-3}, respectively. Fast recombination in the high temperature part of the crystal reduces both concentrations. At a temperature of approximately 1200 K, axial point defect concentrations become stable. Fully coupled transient heat and transient point defect simulations are performed. Figure 4 shows normalized differences between the concentration of interstitials and vacancies. Positive (red) values indicate an excess of interstitials, and negative (blue) values indicate an excess of vacancies. Due to the high pull rate at the beginning, vacancies dominate at the beginning. Due to the convective transport according to the pulling this results in a

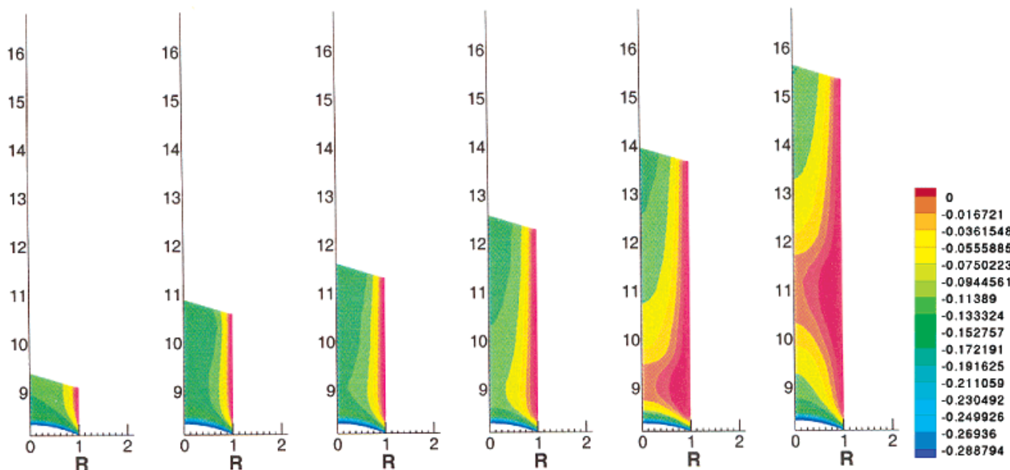

Figure 4. Point defect distribution of crystal at various time steps. Scaled difference $C_i - C_v$.

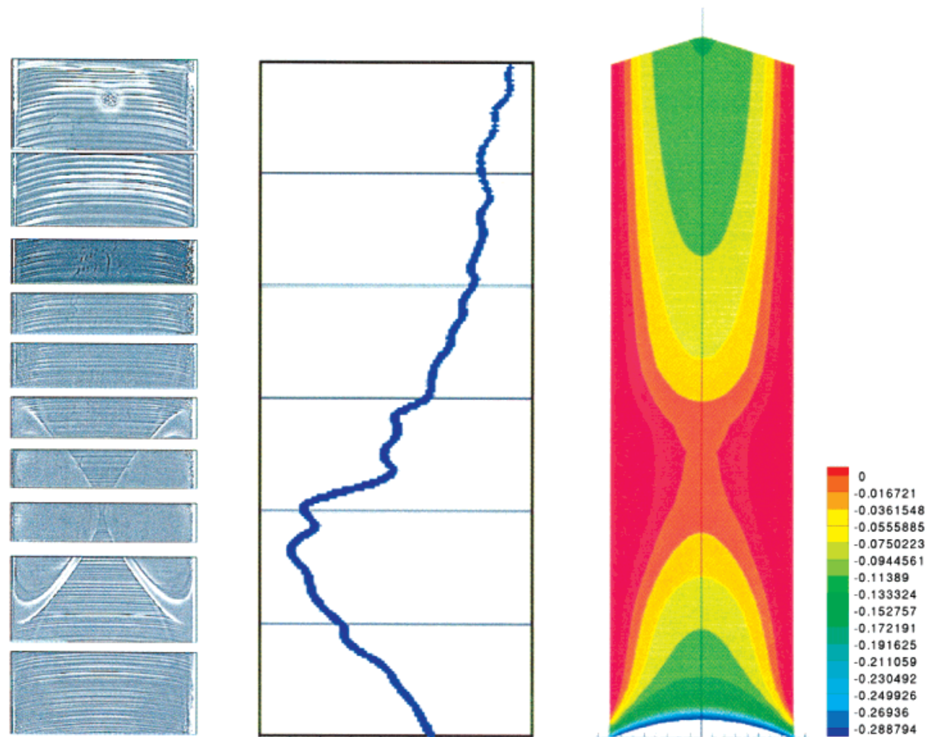

Figure 5. Lifetime map of the axial cut of an as grown crystal, with the simulated deflection of the phase boundary and the point defect concentration.

vacancy-rich upper part of the crystal. As the pull rate decreases, the concentration of interstitials increases and finally dominate. As the pull rate increases, the concentration of vacancies increases again and the interstitial reservoir moves upward with the pull rate. Due to the faster diffusion of interstitials than vacancies, the interstitial reservoir spreads into the vacancy-rich regions. This effect cannot be modeled by a quasi-steady assumption. The v/G law, based on that assumption, can therefore be applied if strong variations in the pulling velocity occur. The high interstitial concentrations at the crystal boundary result from the specified equilibrium concentrations and are overestimated in the simulation results.

Comparison with Experiments. Lifetime maps of an axial cut of an Si crystal grown according to the velocity profile in Figure 1 are shown in Figure 5. Lifetimes are higher in the interstitial-rich region and lower in the vacancy-rich region. The maps clearly show a vacancy/interstial crossover represented by the inner thin light band around the two interstitial-rich regions in the middle. The OSF-ring region is the dark black band between the two light bands. The crystal is vacancy-rich in the upper and lower part and interstitial-rich in the middle. This and also the position of the interstitial-rich region is in good agreement to the simulation results. Remember that the interstitial concentration at the boundary is overestimated due to the underlying model. Besides the defect concentration, the lifetime maps also show the shape of the phase boundary. Here for high pull rates according to the upper and lower part of the crystal the phase boundary is more deflected than in the middle, according to low pull rates. This is in good agreement to our simulation results.

Summary and Conclusions

Coupled transient heat transfer and transient point defect transport have been successfully simulated with varying pull rates for growing silicon crystals. The simulation results coincide qualitatively with experimental lifetime measures and demonstrate that strong variations in the pulling velocity cannot be neglected if point defect distribution in the crystal is a major concern. To predict the concentration of intrinsic point defect in the crystal, the thermal history of the crystal should therefore no longer be neglected.

Acknowledgment. We would like to thank Wacker Siltronic AG for financial support and providing the experimental results.

Nomenclature

ρ_{0i} density of component i
c_{pi} heat capacity of component i
u_i velocity of component i
k_i thermal conductivity of component i
P_i heat source term of component i
T_i temperature of component i
p pressure
σ Stefan–Boltzmann constant
ϵ emissivity
$C_{i,v}$ concentration of interstitials or vacancies
$D_{i,v}$ diffusion coefficients for point defect diffusion
$Q_{i,v}$ activation enthalpy for thermal diffusion of point defects
$C_{i,v}^{eq}$ equilibrium concentrations of interstitials or vacancies
k Boltzmann constant
k_{rec} reaction coefficient for recombination of interstitials or vacancies

References

(1) Dornberger, E. Ph.D. Thesis, Universite Cath. de Louvain, 1997.
(2) Voronkov, V. *J. Cryst. Growth* **1982**, *59*, 625.
(3) Sinno, T. Ph.D. Thesis, MIT, 1999.
(4) Dupret, F.; Nicodeme, P.; Ryckmans, Y.; Wouters, P.; Crochet, M. *Int. J. Heat Mass Transfer* **1990**, *33*, 1849.
(5) Voigt, A. Ph.D. Thesis, Technische Universität München, 2001.
(6) Seidl, A.; Müller, G.; Dornberger, E.; Tomzig, E.; Rexer, B.; von Ammon, W. *Electrochem. Soc. Proc.* **1998**, *98–1*, 417.
(7) Virbulis, J.; Wetzel, T.; Muiznieks, A.; Hanna, B.; Dornberger, E.; Tomzog, E.; Mülbauer, A.; von Ammon, W. *J. Cryst. Growth* **2001**, *230*, 92.
(8) Kurz, M.; Pustai, A.; Müller, G. *J. Cryst. Growth* **1999**, *198/199*, 101.
(9) Järvinen, J. Ph.D. Thesis, University Jyväskylä, 1997.
(10) Dupret, F.; van den Bogaert, N. In *Handbook of Crystal Growth*, 2b; Hurle, D. T. J., Ed.; Elsevier: New York, 1994.
(11) Zhang, H.; Zheng, L. L.; Prasad, V.; Larson, D. J., Jr. *J. Heat Transfer* **1998**, *120*, 874.
(12) Voigt, A.; Hoffmann, K.-H. *Int. Ser. Num. Math.* **2001**, *139*, 259.
(13) Dornberger, E.; von Ammon, W.; Virbulis, J.; Hanna, B.; Sinno, T. *J. Cryst. Growth* **2001**, *230*, 291.

CG034005U